




Article

Comparison of Lead-Acid and Li-Ion Batteries Lifetime Prediction Models in Stand-Alone Photovoltaic Systems

Rodolfo Dufo-López ^{1,*} , Tomás Cortés-Arcos ², Jesús Sergio Artal-Sevil ¹  and José L. Bernal-Agustín ¹ 

¹ Departamento de Ingeniería Eléctrica, Universidad de Zaragoza, C/María de Luna, 3, 50018 Zaragoza, Spain; jsartal@unizar.es (J.S.A.-S.); jlbernal@unizar.es (J.L.B.-A.)

² Escuela Universitaria Politécnica de La Almunia, EUPLA, Universidad de Zaragoza, C/Mayor, s/n, La Almunia, 50100 Zaragoza, Spain; tcortes@unizar.es

* Correspondence: rdufo@unizar.es

Abstract: Several models for estimating the lifetimes of lead-acid and Li-ion (LiFePO₄) batteries are analyzed and applied to a photovoltaic (PV)-battery standalone system. This kind of system usually includes a battery bank sized for 2.5 autonomy days or more. The results obtained by each model in different locations with very different average temperatures are compared. Two different locations have been considered: the Pyrenees mountains in Spain and Tindouf in Algeria. Classical battery aging models (equivalent full cycles model and rainflow cycle count model) generally used by researchers and software tools are not adequate as they overestimate the battery life in all cases. For OPzS lead-acid batteries, an advanced weighted Ah-throughput model is necessary to correctly estimate its lifetime, obtaining a battery life of roughly 12 years for the Pyrenees and around 5 years for the case Tindouf. For Li-ion batteries, both the cycle and calendar aging must be considered, obtaining more than 20 years of battery life estimation for the Pyrenees and 13 years for Tindouf. In the cases studied, the lifetime of LiFePO₄ batteries is around two times the OPzS lifetime. As nowadays the cost of LiFePO₄ batteries is around two times the OPzS ones, Li-ion batteries can be competitive with OPzS batteries in PV-battery standalone systems.

Keywords: lead-acid batteries; lithium batteries; photovoltaic; standalone systems; battery lifetime



Citation: Dufo-López, R.; Cortés-Arcos, T.; Artal-Sevil, J.S.; Bernal-Agustín, J.L. Comparison of Lead-Acid and Li-Ion Batteries Lifetime Prediction Models in Stand-Alone Photovoltaic Systems. *Appl. Sci.* **2021**, *11*, 1099. <https://doi.org/10.3390/app11031099>

Academic Editor: Roberto Saletti

Received: 17 November 2020

Accepted: 21 January 2021

Published: 25 January 2021

Publisher's Note: MDPI stays neutral with regard to jurisdictional claims in published maps and institutional affiliations.



Copyright: © 2021 by the authors. Licensee MDPI, Basel, Switzerland. This article is an open access article distributed under the terms and conditions of the Creative Commons Attribution (CC BY) license (<https://creativecommons.org/licenses/by/4.0/>).

1. Introduction

Renewable electricity generation is widely used in rural areas where the electrical grid is weak or nonexistent. Stand-alone (off-grid) systems are typically powered by a photovoltaic (PV) generator with battery storage. In this kind of system, the battery technology most widely used is lead-acid. In some cases, a hybrid PV–fossil fuel generator (diesel or gasoline)–battery storage system can be optimal—that is, the system with lower costs during the system's lifetime. Standalone systems can be direct current (DC) or altern current (AC) coupled [1]—that is, the bus where components are connected can be the DC bus or the AC bus. DC coupled systems (Figure 1) are usual in low power systems (typically lower than 5 kW), while the AC-coupled system is commonly used in larger systems. The charge controller is needed to avoid overcharge and over-discharge of the battery, preventing premature failure. Additionally, an inverter (DC/AC) is needed when there is AC load.

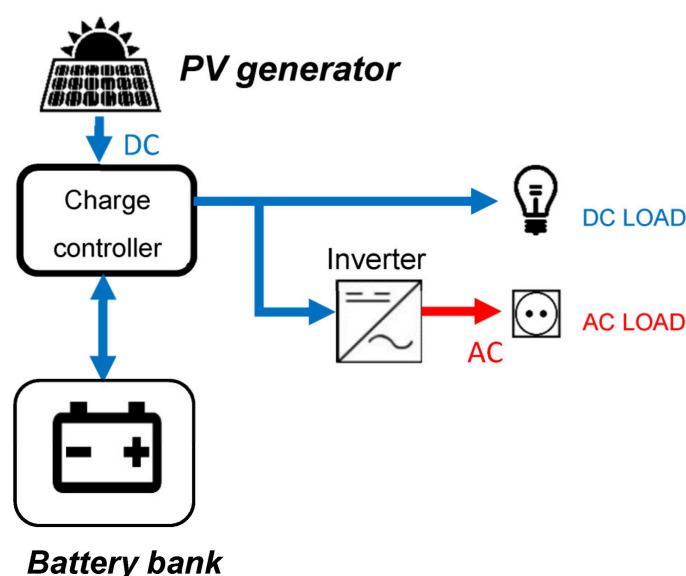


Figure 1. Direct current (DC) coupled standalone photovoltaic (PV) system.

In standalone systems, different types of batteries can be used [2]. Lead-acid batteries (valve-regulated lead-acid type, VRLA) are the dominant technology for photovoltaic off-grid applications [3] due to their affordable costs for large installed capacities. However, lead-acid batteries are the overall weakness of the PV system and tend to be replaced by new technologies such as Li-ion batteries [4], which can be competitive in some cases [5] due to their higher cycle life, despite their higher cost.

The total battery cost (including its replacement during the system lifetime) is the highest in the system's net present cost (NPC); thus, in the optimization process of standalone systems, the accurate estimation of battery life is one of the most critical issues. Significant errors in the battery lifetime prediction would lead to great errors in the estimation of the NPC.

Lead-acid battery aging factors are charge and discharge rates, charge (Ah) throughput, the time between full charge, time at a low state of charge (SOC), and partial cycling. Several researchers have analyzed the lead-acid battery aging factors [6,7]. Classical models widely used by researchers and software tools to estimate the battery life are the "equivalent full cycles model" and the "rainflow cycle counting model" [8].

The equivalent full cycles model counts the full charge (Ah throughput) cycled by the battery since the start of its lifetime, without considering SOC, temperature, current, or any other variable; when this value reaches the charge, the battery can cycle, considering the cycle life shown in the manufacturer datasheet obtained under standard tests, and the end of the battery life is reached. The rainflow cycle count model includes the effect of the depth of discharge (DOD). Nevertheless, real operating conditions (current rate, temperature, DOD, SOC, etc.) are different from the laboratory conditions of the cycles shown by the manufacturer datasheet, so a significant error in the lifetime prediction can be obtained.

Most of the previously published studies of the simulation and/or optimization of systems with battery systems do not use advanced models to estimate battery lifetime. In many cases, the battery degradation is not considered or its lifetime is estimated in fixed values based on the experience of the researcher [9–20]. In other cases, battery lifetime is estimated by using the equivalent full cycles model [21–25]. In the best cases, it may be estimated by using the rainflow cycle counting method [26–29]. However, a battery's real lifetime can differ from the estimated lifetime by many years using the mentioned methods, depending on the operating conditions. As previously mentioned, a high error in the estimation of the battery life would imply a great error in the estimation of the total

cost of the batteries in the NPC of the system; therefore, the real levelized cost of Energy (LCE) may be very different from the expectation.

A much more accurate lead-acid aging model (and also more complex and with higher computational difficulty) is the one described by Schiffer et al. [30], called “weighted *Ah* throughput model” and used by iHOGA software [31]. The model is based on applying weighting factors for the battery’s charge throughput to estimate the lost capacity (considering the different stress factors for cycling and corrosion). Schiffer et al.’s model was used to estimate the battery life in PV systems [32,33]. This model obtained results very similar to the real ones [33], while the equivalent full cycles model and the cycle counting model obtained lifetime estimations that can be, in some cases (PV-battery systems), two or three times higher than the real battery lifetime.

Li-ion batteries ([34–36]) have a higher cycle life, energy density, and energy efficiency, and lower maintenance compared to lead-acid batteries. The LiFePO_4 (LFP) type is the most used in off-grid systems. Li-ion batteries’ most significant aging external factors are temperature, charge and discharge rates, and DOD [37]. In simulation and optimization of standalone systems, Li-ion cell level aging models [38] are usually used due to their simplicity. Electrochemical models are usually very complex, even the most simplified ones [37,39,40], implying high calculation times [41]. “Calendar” aging occurs when a battery is not being used while “cycle” aging occurs when the battery is under charge or discharge current [41]. Cycle aging is affected by the total charge (*Ah*) throughput from the start of battery lifetime, the current, the ambient temperature, and the SOC. Calendar aging main factors are temperature and SOC [38]. A good example of Li-ion aging model text matrix is shown in the work of Oyarbide et al. [42].

The rainflow cycle count model is also used for Li-ion batteries. Arrhenius kinetic-based aging models [38] are the most used cycle aging models for Li-ion batteries. For example, Wang et al.’s [43] model was obtained by performing many accelerated cycling tests to commercial LiFePO_4 cells, obtaining a capacity fade model that takes into account the *Ah*-throughput and temperature for different charge/discharge rates. Li-ion battery calendar aging has been modeled by different researchers [38]. For example, Petit et al. [44] used an expression based on Arrhenius law, considering temperature, time, and SOC.

In this work, we compare the battery lifetime estimation of a PV-battery system used to supply electricity to a household located in two different locations with very different average temperatures, considering different models for the degradation of lead-acid or Li-ion batteries. In Section 2, the models of the PV system components and the different battery lifetime models are shown. In Section 3, we show the comparison of the different models applied in the PV-battery systems. Finally, the main findings and conclusions are discussed in Section 4.

2. Materials and Methods

In this section, the components’ models are described, emphasizing the different battery lifetime models used. The system’s simulation was performed over the course of a whole year in hourly intervals ($t = 0 \dots 8760$ h), and the results were extrapolated for the remaining years of the system’s lifetime.

2.1. Photovoltaic Generator

If there was no maximum power point tracking in the controller (typical in DC-coupled systems), the PV output current during time t , $I_{PV}(t)$ (A), was calculated as follows ([33]), where the effect of the module temperature is negligible:

$$I_{PV}(t) = I_{SC} \cdot G(t) \quad (1)$$

where I_{SC} is the shortcut current (A) of the PV module and $G(t)$ (kW/m^2) is the irradiance over the module surface at time t .

The output power of the PV generator (W) of N_{PV_p} strings in parallel was obtained by using Equation (2):

$$P_{PV}(t) = N_{PV_p} \cdot I_{PV}(t) \cdot V_{DC}(t) \cdot f_{PV_loss} \quad (2)$$

where $V_{DC}(t)$ (V) is the battery bank voltage in DC-coupled systems and f_{PV_loss} is the loss factor (PV module mismatch or power tolerance, losses due to dirt in the PV modules, and losses in the wires).

2.2. Charge Controller

It prevents overcharge and over-discharge of the battery. In lead-acid batteries, overcharge is avoided by charging batteries in three stages (bulk, absorption, or boost and float stages, Figure 2). Absorption includes battery equalization in some cycles, periodically. During the second and third stages, the current is limited using the pulse with modulation (PWM) technique. The limits between stages are voltage setpoints, while advanced controllers compare the minimum battery state of charge (SOC) of the previous discharge with SOC setpoints to determine the charge stages to be applied. In this work, SOC controllers performed the boosting stage if the SOC during the last discharge was lower than a specific value (usually 70%), and equalization was performed if battery SOC during discharge was lower than another specific value (usually 40%).

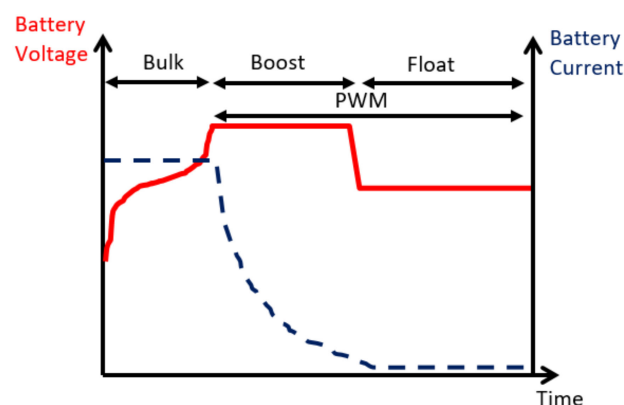


Figure 2. Charge controller charging stages.

Lithium batteries require a specific charge controller, as there is a very little voltage difference for a high SOC difference (state of function is estimated in Li-ion batteries), and they cannot accept overcharge; therefore, there is no equalization stage and no float stage, just a constant voltage/constant current (CV/CC) charge algorithm. Some controller models are programmable and can be used for lead-acid or for lithium batteries.

The charge controller prevents over-discharge by disconnecting the battery when a specific setpoint voltage (or SOC) is reached and reconnecting after partial recharging when another higher specific setpoint voltage (or SOC) is reached.

2.3. Inverter

Although charge controllers include battery over-discharge protection, standalone inverters also include this feature (in some cases, they are directly connected to the battery). The inverter efficiency depends on its output power, as shown in Figure 3. Many researchers and software tools use a constant value for the inverter efficiency, leading to significant errors when the AC load profile has great peaks and valleys.

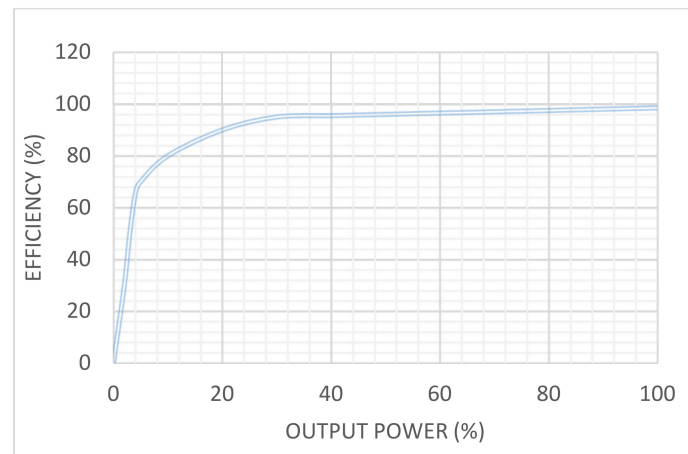


Figure 3. Typical inverter efficiency [45].

2.4. Battery

During each time step, the state of charge $SOC(t)$ (per unit) was calculated from the previous time step SOC , adding or subtracting the charge of the battery current:

$$SOC(t) = SOC(t - \Delta t) + \int_{t-\Delta t}^t \frac{I_b(\tau)}{C_N} d\tau \quad (3)$$

where Δt is the length of the time step (h), $I_b(t)$ (Equation (4)) is the current that effectively affects the battery charge, C_N is the nominal capacity of the battery (Ah), and τ is the time between $t - \Delta t$ and t .

$$I_b(t) = I_{bat}(t) \cdot \eta_{bat_ch}; I_{bat}(t) > 0 \text{ (charge)} \\ I_b(t) = \frac{I_{bat}(t)}{\eta_{bat_d}}; I_{bat}(t) < 0 \text{ (discharge)} \quad (4)$$

where $I_{bat}(t)$ (positive charging, negative discharging) is the battery current, η_{bat_ch} is the charging efficiency, and η_{bat_d} is the discharging efficiency. Usually both efficiencies are considered to be the same, equal to the square root of the roundtrip efficiency.

Battery degradation models are shown in the next subsections. In all the models, if the battery lifetime estimation in years was higher than the floating life (shown in the manufacturer datasheet), the floating life was used as the battery lifetime. In the upcoming subsections, the battery voltage will be modelled.

2.4.1. Equivalent Full Cycles Model

This method estimates the end of the battery lifetime when a specified number of full charge–discharge cycles (regardless of the operating conditions) are reached (Z_{IEC}), defined by the IEC standard [46].

During the simulation, for every time step, the equivalent number of full cycles since the beginning (Z_N) was calculated as follows:

$$Z_N(t + \Delta t) = Z_N(t) + \frac{|I_b(t)| \cdot \Delta t}{C_N} \quad (5)$$

where $|I_b(t)|$ is the absolute value of the discharge current. When $Z_N(t) = Z_{IEC}$, the end of the lifetime of the battery has been reached.

2.4.2. Rainflow Cycles Counting Model

This model is more complex and precise as it considers the depth of discharge (DOD) of the charge/discharge cycle, and is based on Downing's algorithm [47]. This method is based on counting, during one year of the system's simulation, the charge/discharge cycles

Z_i corresponding to each range of the DOD (split into m intervals). There are a number of cycles to failure (CF_i) obtained from the manufacturer datasheet (Figure 4).

Battery duration, in years, can be calculated as follows:

$$Life_b = \frac{1}{\sum_{i=1}^m \frac{Z_i}{CF_i}} \quad (6)$$

Cycles to Failure

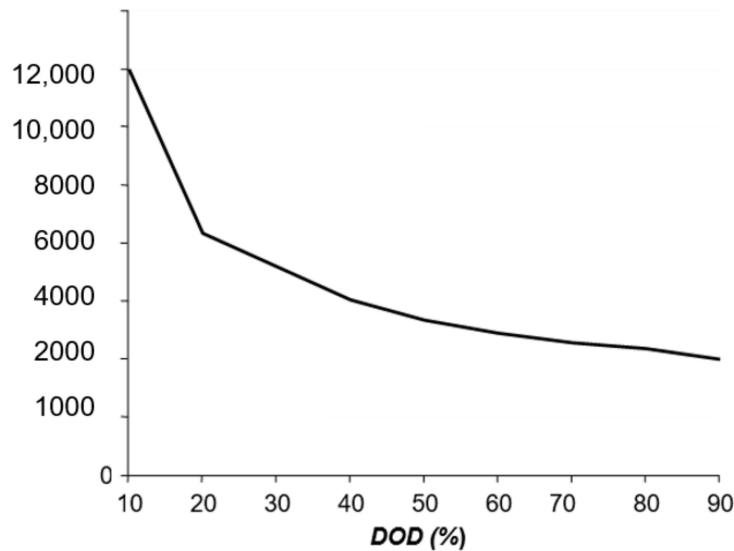


Figure 4. Lead-acid battery: cycles to failure vs. depth of discharge (DOD) [48].

2.4.3. Lead-Acid Batteries: Schiffer et al.'s Weighted Ah-Throughput Model

The weighted Ah-throughput model presented by Schiffer et al. [30] assumes that operating conditions are typically more severe than those used in standard tests of cycling and float lifetime.

This model uses weighting factors for the charge throughput over the battery life to model the lost capacity due to the different aging mechanisms. These weights depend on the DOD, the current rate, the acid stratification, and the time since the last full charging.

Battery voltage at each time step was calculated depending on if the battery was $I_{bat}(t) > 0$ (charging), Equation (7), or $I_{bat}(t) < 0$ (discharging), Equation (8), using the Shepherd model [49]:

$$V_b(t) = V_0 - gDOD(t) + \rho_c(t) \left(\frac{I_{bat}(t)}{C_N} \right) + \rho_c(t) M_c \left(\frac{I_{bat}(t)}{C_N} \right) \left(\frac{SOC(t)}{C_c - SOC(t)} \right) \quad (7)$$

$$V_b(t) = V_0 - gDOD(t) + \rho_d(t) \left(\frac{I_{bat}(t)}{C_N} \right) + \rho_d(t) M_d \left(\frac{I_{bat}(t)}{C_N} \right) \left(\frac{DOD(t)}{C_d(t) - DOD(t)} \right) \quad (8)$$

where V_0 (V) is the open-circuit equilibrium cell voltage at the fully charged state, g (V) is an electrolyte proportionality constant, $\rho_c(t)$ and $\rho_d(t)$ (Ω Ah) represent the aggregated internal resistance during charge or discharge, and C_c and $C_d(t)$ represent the normalized capacity of the battery during charge or discharge.

This model estimates the capacity loss by corrosion, $\Delta C^c(t)$ and the capacity loss by cycling (degradation), $\Delta C^d(t)$. Each hour, the remaining battery capacity, $C_{rem}(t)$, could be estimated as the normalised initial battery capacity $C_d(0)$ minus the capacity loss by corrosion and degradation. The end of the battery life was considered to be when $C_d(t) = 0.8 C_N$.

$$C_{rem}(t) = C_d(0) - \Delta C^c(t) - \Delta C^d(t) \quad (9)$$

Capacity loss by degradation $\Delta C^d(t)$ was calculated counting the weighted number of cycles, with the impact of the SOC, the discharge current, and the acid stratification. At the same time, the capacity loss by corrosion was estimated, which is proportional to the effective corrosion layer thickness, which grows during the lifetime of the battery depending on the corrosion voltage of the positive electrode and temperature. This is a complex model with many equations; further details can be found in [30].

2.4.4. LFP Li-Ion Models

In Li-ion batteries, during each time step, the capacity loss $Q(t)$ (percentage capacity fade) can be calculated as the sum of cycle capacity fade and calendar capacity fade:

$$Q(t) = Q_{cal}(t) + Q_{cyc}(t) \quad (10)$$

Cycle capacity fade is affected by the charge cycled, which depends on the number of cycles N and DOD , and it is also affected by other factors such as SOC, current and ambient temperature T . Calendar aging depends on the temperature, SOC, and time t [38].

Different models can calculate the cycling capacity fade. Electrochemical models are usually very complex. One of the most simplified electrochemical models is Astaneh et al.'s Li-ion battery lifetime prediction model [37,39], which integrates the simplified single particle model (SSPM) and reduced-order model (ROM) to predict solid electrolyte interphase growth (SEI), giving good results for moderate cycling currents; however, it includes many variables that are dependent on the specific chemistry of the battery and are difficult to estimate.

It must be settled that each aging model is intrinsically related to each cell type and, therefore, the same aging model cannot be valid for all the Li-ion models.

Wang et al.'s Cycle Aging Model

Wang et al. [43] obtained the cycle capacity fade for commercially available 2.2 Ah cells from A123 Systems, for different C-rates and temperatures:

$$Q_{cyc}(t) = B \cdot \exp \left[\frac{-31700 + 370.3 \cdot C_{rate}}{RT} \right] (Ah)^{0.55} \quad (11)$$

where B is the pre-exponential factor that depends on C_{rate} (h^{-1}) (current through the battery in A divided by its nominal rated capacity in Ah), R is the gas constant (8.314 J/mol-K), and T is the ambient temperature (K). $Ah = N \cdot DOD \cdot C_N$ is the total Ampere-hour (Ah) throughput of the battery.

Groot et al.'s Cycle Aging Model

Groot et al. [50] model was obtained after testing commercial LFP cells for different currents I (A) and temperatures T ($^{\circ}C$):

$$Q_{cyc}(t) = a \cdot e^{b \cdot I \cdot T^c \cdot I^2 + d \cdot I + e} + f \quad (12)$$

where a , b , c , d , e , and f are fit parameters.

Petit et al.'s Calendar Aging Model

Calendar capacity fade is modelled by Petit et al. [44] using an expression based on Arrhenius law, dependent on temperature, time, and SOC:

$$Q_{cal}(t) = B_{cal}(SOC) \cdot \exp \left[\frac{-E_{a_cal}(SOC)}{RT} \right] t^{z_{cal}(SOC)} \quad (13)$$

where $B_{cal}(SOC)$ (Ah/s ^{Z_{cal}}) is the pre-exponential factor depending on SOC, $E_{a_{cal}}(SOC)$ is the activation energy (Jmol⁻¹), and $z_{cal}(SOC)$ is a dimensionless constant (assumed to be a value of 0.5).

Wang et al.'s Calendar Aging Model Combined with Petit et al.'s Calendar Model

Cycle aging mainly occurs when the battery is charging. Petit et al. [44] postulates that it only happens when the current is above a given limit I_{limit} (A), using in this case the Wang model, while when current is lower than the limit calendar aging occurs, using, in said case, Equation (13). The limit current depends on the battery capacity to tackle high charging rates.

3. Results

An off-grid household AC load profile from a previous publication [33] has been considered to compare the battery lifetime estimation of the PV-battery system. The average measured AC load was 3.61 kWh/day. The system is located in the Pyrenees mountains, in Aragon, Spain (latitude 42.772°, longitude -0.334°) with an average outdoor annual temperature of 5.1 °C. For comparison, the same system is considered to be in a desertic place (Tinduf, Argelia, latitude 27.669°, longitude -8.144°), with an average outdoor annual temperature of 23.1 °C.

Different battery lifetime estimation models will be used.

For lead-acid batteries:

- Equivalent full cycles model;
- Rainflow cycle count model;
- Schiffer et al.'s weighted Ah-throughput model.

For LiFePO₄ batteries:

- Equivalent full cycles model;
- Groot et al.'s cycle aging model.

Wang et al.'s calendar aging model combined with Petit et al.'s calendar model considered an I_{limit} of 5% of the battery bank's nominal capacity (that is, current at C-rate of 20 h, C20).

The nominal voltages are 48 VDC and 230 VAC.

The PV modules considered have a peak power of 100 W, 12 V nominal voltage, and short-circuit current of 6.79 A. In the Pyrenees, the PV generator is composed of four serial × seven parallel PV modules (total 2800 W), while in Tindouf (higher irradiation) it is composed of four serial × six parallel PV modules (total 2400 W). A loss factor of $f_{PV_loss} = 0.8$ was considered.

Two types of battery banks were considered for both locations. The battery bank size was selected, considering that about 2.5 days of autonomy are required.

- The lead-acid battery bank, which consists of 24 × 2 V OPzS [30] (flooded, tubular-plated, deep cycle) commercial batteries in serial, $C_N = 270$ Ah (total 12.96 kWh), 1258 equivalent full cycles (CF vs. DOD curve shown in Figure 4), float life of 20 years at 20 °C (manufacturer datasheet) and roundtrip efficiency of 85%. SOC to disconnect load (SOC_{min}) 20%. The parameters for the Schiffer model were the ones used in [30].
- Li-ion LFP battery consists of a commercial 48 V pack of $C_N = 213.3$ Ah (total 10.24 kWh), 5600 cycles at 80% DOD, 4022 equivalent full cycles, float life of 20 years at 20 °C (manufacturer datasheet does not show float life, but operating life of 20 years for stationary battery systems is usually considered [51]) and roundtrip efficiency of 90%. SOC_{min} is 10%.

The nominal inverter power is 600 W, and its efficiency is shown in Figure 3.

The annual average ambient temperature in the battery room in the Pyrenees location was estimated to be higher than the outdoor temperature. We considered two values as the average: 8 or 12 °C. In the desertic place of Tindouf, we considered that in the battery room, the average temperature can be similar to the average outdoor temperature, 23.1 °C.

Considering Arrhenius law, corrected float life at the different temperatures considered are shown in Table 1.

Table 1. Float life at different temperatures considering Arrhenius law.

	Standard	Pyrenees		Tinduf
Average temperature (°C)	20	8	12	23.1
Battery float life (years)	20	46.1	35.1	16.1

Irradiation over the optimal slope (south orientation) for both locations is shown in Table 2.

Table 2. Monthly average irradiation data from Photovoltaic Geographical Information System (PVGIS) [52], year 2015.

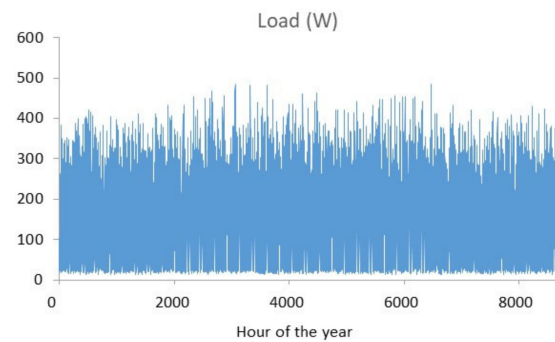
	Jan.	Feb.	Mar.	Apr.	May	Jun.	Jul.	Aug.	Sep.	Oct.	Nov.	Dec.
Pyrenees, 65° slope irradiation (kWh/m ² /day)	3.31	2.69	3.92	4.71	4.76	4.49	5.03	5.17	4.93	3.87	3.68	3.87
Tinduf, 35° slope irradiation (kWh/m ² /day)	6.75	7.54	7.7	7.41	7.36	7.02	6.65	6.5	6.64	5.85	7.07	6.43

Table 3 shows the results of the simulation during a whole year for the two locations considered. It can be seen that the battery bank charge/discharge energy is very low (roughly 700 kWh/yr), which implies around 60 equivalent full cycles. The charge/discharge rates are very low, as is usual in PV-battery stand-alone systems: the average charge rate is roughly 4% of the battery's nominal capacity, while the average discharge rate is around 1%.

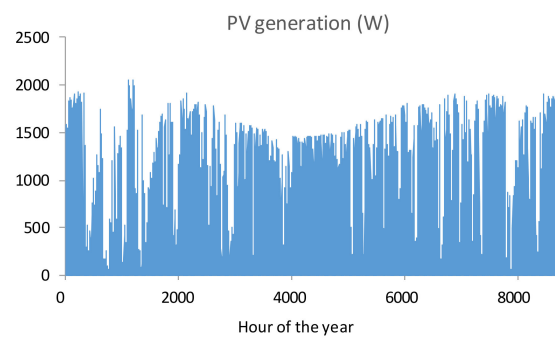
Table 3. Results of the simulation during a whole year for the different systems.

Battery Type	Pyrenees		Tindouf	
	Lead-acid	Li-ion	Lead-acid	Li-ion
Load (kWh/yr)	1318	1318	1318	1318
PV generation (kWh/yr)	2804	2804	3944	3944
Battery charge/discharge energy (kWh/yr)	740	717	767	669
Equivalent full cycles per year	57.1	70	53.6	65.3
Hours of battery charge per year	2261	2151	3102	2399
Hours of battery discharge per year	5757	5792	5050	5050
Average charge rate (% of C _N)	3.77	4.67	4.15	4.88
Average discharge rate (% of C _N)	0.97	1.23	1.03	1.30

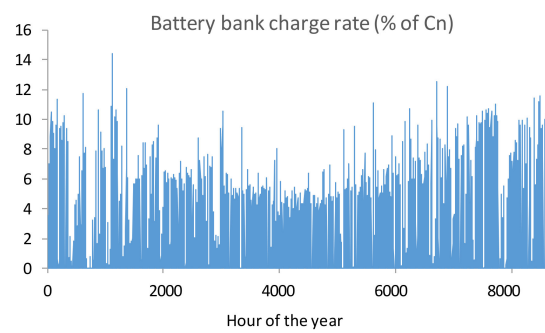
The hourly simulation of a whole year is shown in Figure 5 (Pyrenees, lead-acid) and 6 (Tindouf, Li-ion). For Tindouf, the battery bank is almost all the time at SOC higher than 80% (Figure 6). For the Pyrenees, the battery bank is also most of the time at higher SOC than 80%; however, in winter, there are periods with lower SOC (Figure 5), reaching 30% during short periods.



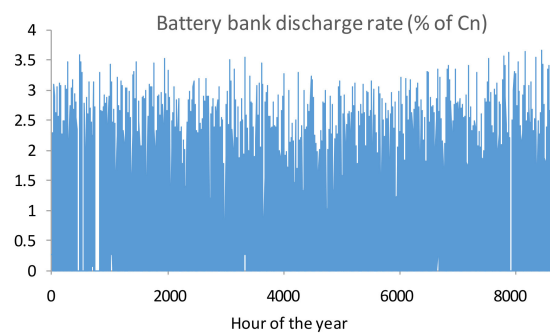
(a)



(b)



(c)



(d)

Figure 5. Cont.

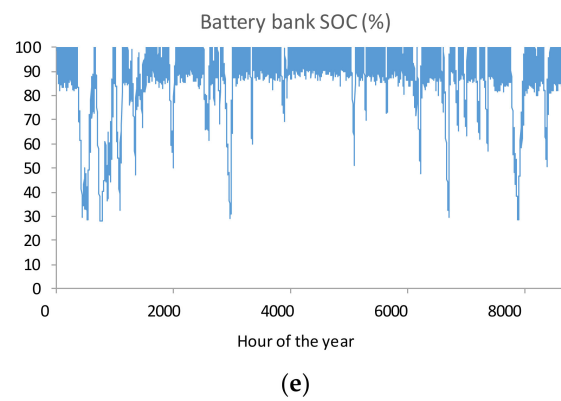


Figure 5. Hourly simulation of the Pyrenees—lead-acid battery: load (W) (a), PV generation (W) (b), battery bank discharge rate (% of Cn) (c), charge rate (% of Cn) (d) and state of charge (SOC) (%) (e).

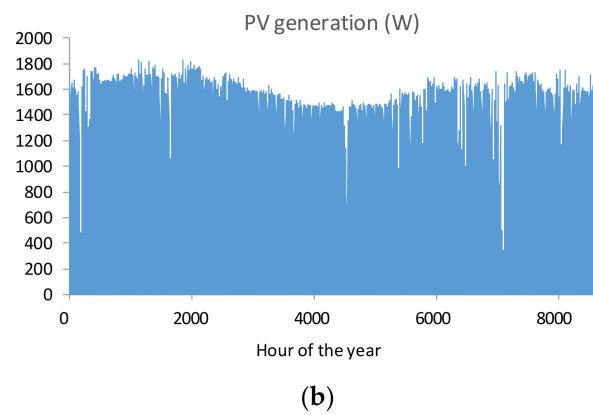
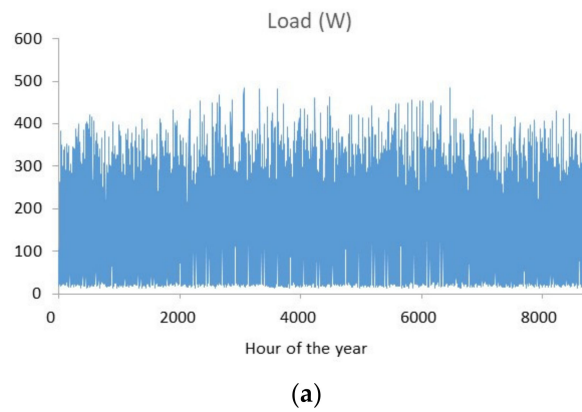


Figure 6. *Cont.*

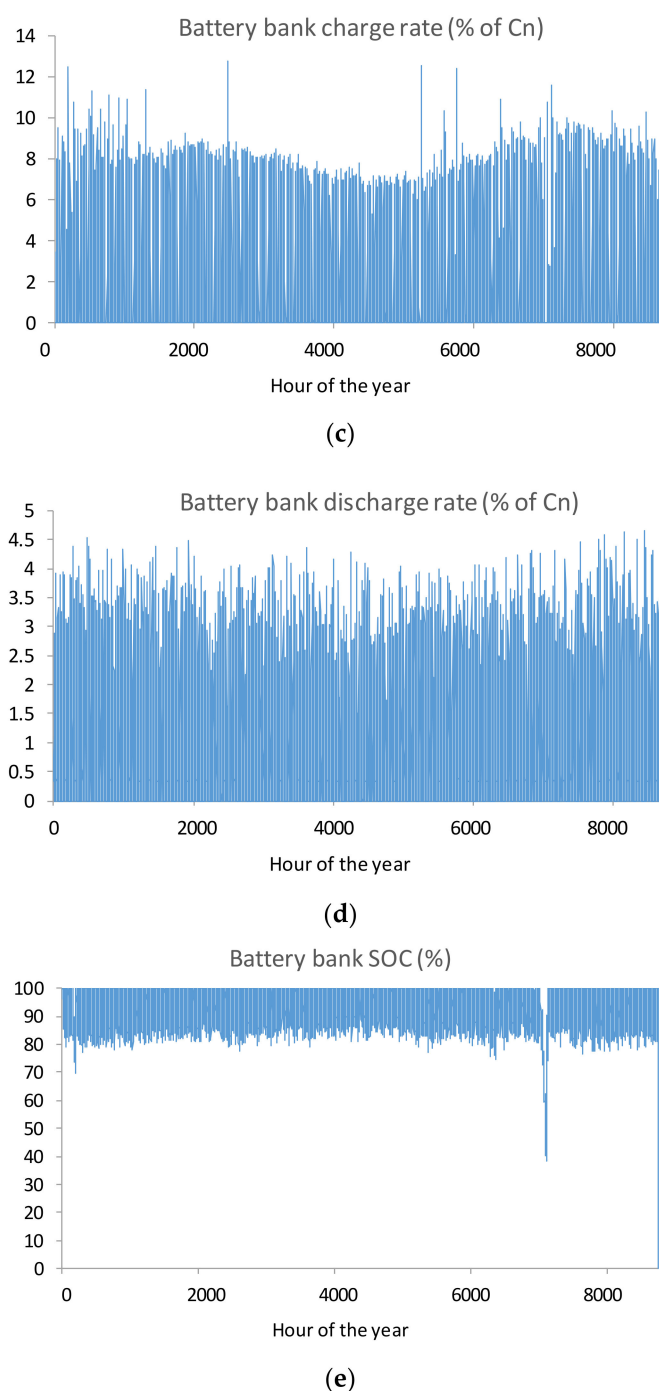


Figure 6. Hourly simulation of Tindouf—Li-ion battery: load (W) (a), PV generation (W) (b), battery bank discharge rate (% of Cn) (c), charge rate (% of Cn) (d) and SOC (%) (e).

The estimated battery lifetimes obtained by the different models are shown in Table 4 (lead-acid) and Table 5 (Li-ion).

Table 4. Results. Battery lifetime estimation (years) for lead-acid batteries.

	Eq. Full Cycles	Rainflow	Schiffer	Value Selected
Pyrenees 8 °C	22.7	24.2	12.2	12.2
Pyrenees 12 °C	22.7	24.2	11.8	11.8
Tinduf 23.1 °C	23.0	26.8	4.8	4.8

Table 5. Results. Battery lifetime estimation (years) for Li-ion batteries.

	Eq. Full Cycles	Groot	Wang + Petit	Value Selected
Pyrenees 8 °C	67.2	162.1	66.5	20
Pyrenees 12 °C	67.2	141.1	41.4	20
Tinduf 23.1 °C	68.9	118.2	13.7	13.7

For the Pyrenees and lead-acid batteries (Table 4), lifetime estimation using the equivalent full cycles model or rainflow model is higher than float life at 20° (20 years) but lower than expected float lifetime considering temperature (Table 1). For Tindouf and lead-acid, both models obtained values much higher than the expected float life. However, the more accurate Schiffer model obtained values much lower than the expected float life, and these results are the selected ones (marked in green in Table 4).

For the Pyrenees and Li-ion batteries (Table 5), all the models obtained values much higher than the float life at the average temperature considered. The selected values are 20 years, marked in green in Table 4, as it is the value usually considered for stationary battery systems, although at low temperatures than 20 °C higher lifetimes could be achieved [51]. For Tindouf and Li-ion, the equivalent full cycles model and Groot model obtained overestimated values, as they do not consider the calendar aging. The only model that is considered correct is Wang–Petit, as it is the only one that considers calendar aging, which has great importance in standalone systems, with very low charge/discharge rates.

The results were not verified, as extensive time and resources would have been needed to conduct Li-ion aging tests and to verify the aging models. In this work, we wanted to estimate the lifetime of the battery using several available models. To obtain the tuning parameters of the different models, Li-ion batteries should be tested under similar conditions as the working conditions, during several years, as working conditions in standalone PV systems are low current (usually lower than C/20) and take many hours during the day at floating stage. This was not possible if we wanted to make the prediction now, so the available models were used. Usually, researchers and engineers use the equivalent full cycles model, but the results show that in many cases (most of the typical stand-alone PV systems) it leads to overestimation of the battery lifetime.

4. Discussion

Considering the typical PV-battery standalone systems, with large battery banks with enough energy to supply more than 2 days of autonomy (in many cases 3 or 4 days, or even more), the charge/discharge rates were very low, typically around C20 (current in A roughly 5% of the nominal capacity in Ah).

In these cases, for lead-acid batteries, the equivalent full cycles model or the rainflow cycle counting model overestimated the battery lifetime, being necessary to use Schiffer et al.'s [30] model, obtaining in the case studied a lifetime of roughly 12 years for the Pyrenees and 5 years for Tindouf.

Using Li-ion batteries, models that just consider cycle aging are not correct—it is necessary to consider both cycle and calendar aging, as the model of Wang et al. [43] combined with the calendar aging model of Petit et al. does [44]. For the studied standalone PV-battery system with Li-ion batteries and low temperatures (much lower than 20 °C), the typical value of 20 years for stationary battery systems can be considered as the battery lifetime. However, if the average temperature is higher than 20 °C (as in Tindouf), the battery life is significantly reduced to 13.7 years.

Summarizing, comparing a similar battery bank size in a PV-battery standalone system, the LiFePO₄ battery life is expected to be around two times the OPzS lead-acid one. As the LiFePO₄ battery cost at the end of 2020 can be around two times the OPzS cost, this means that economically LiFePO₄ batteries can be competitive with the OPzS technology. Considering the expected reduction in Li-ion battery cost, we can expect that Li-ion batteries will be widely installed in PV-battery standalone systems in a few years.

Author Contributions: Conceptualization, R.D.-L.; methodology, R.D.-L. and T.C.-A.; software, R.D.-L.; validation, J.S.A.-S., T.C.-A. and R.D.-L.; formal analysis, J.L.B.-A. and R.D.-L.; investigation, R.D.-L. and T.C.-A.; resources, J.S.A.-S. and J.L.B.-A.; data curation, T.C.-A. and R.D.-L.; writing—original draft preparation, R.D.-L. and T.C.-A.; writing—review and editing, J.S.A.-S., R.D.-L. and J.L.B.-A.; visualization, R.D.-L. and T.C.-A.; supervision, R.D.-L. and J.L.B.-A. All authors have read and agreed to the published version of the manuscript.

Funding: This work was supported by the Universidad de Zaragoza programme “Proyectos de investigación–proyectos puente–convocatoria 2019”, project “Modelos de envejecimiento de baterías de litio para su aplicación en simulación y optimización de sistemas aislados de la red eléctrica” [grant number: UZ2020-TEC03].

Institutional Review Board Statement: Not applicable.

Informed Consent Statement: Not applicable.

Data Availability Statement: Data available on request.

Conflicts of Interest: The authors declare no conflict of interest.

Abbreviations

$B_{cal}(SOC)$	Pre-exponential factor depending on SOC (Ah/s ^{Z_{cal}})
C_N	Nominal capacity of the battery (Ah)
C_c	Normalized capacity of the battery during charge (per unit)
$C_d(0)$	Normalized initial battery capacity (Ah)
$C_d(t)$	Normalized capacity of the battery during discharge (per unit)
C_{rate}	Current through the battery divided by its nominal rated capacity (h ^{−1})
$C_{rem}(t)$	Remaining battery capacity (Ah)
DOD	Depth of discharge (%)
$E_{a_{cal}}(SOC)$	Activation energy depending on SOC (Jmol ^{−1})
f_{PV_loss}	PV loss factor
g	Electrolyte proportionality constant (V)
$G(t)$	Irradiance over the module surface at time t (kW/m ²)
$I_b(t)$	Current that effectively affects the battery charge (A)
$I_{bat}(t)$	Battery current (positive charging, negative discharging)
I_{limit}	Limit current above which only cycling degradation is considered (A)
$I_{PV}(t)$	PV output current during time t (A)
I_{SC}	Shortcut current of the PV module (A)
N	Number of cycles
N_{PV_p}	Number of PV strings in parallel
$P_{PV}(t)$	Output power of the PV generator (W)
$Q(t)$	Capacity loss (%)
$Q_{cal}(t)$	Calendar capacity fade (%)
$Q_{cyc}(t)$	Cycle capacity fade (%)
R	Gas constant (8.314 J/mol-K)
$SOC(t)$	State of Charge of the battery (per unit)
t	Time (hour)
T	Ambient temperature (K)
$V_{DC}(t)$	DC bus voltage (V)
V_0	Open-circuit equilibrium cell voltage at the fully charged state (V)
$z_{cal}(SOC)$	Dimensionless constant (assumed a value of 0.5).
Z_{IEC}	Number of full charge-discharge cycles defined by the IEC standard
Z_N	Equivalent number of full cycles since the beginning
$\Delta C^c(t)$	Capacity loss by corrosion (Ah)
$\Delta C^d(t)$	Capacity loss by cycling (degradation) (Ah)

Δt	Length of the time step (h)
η_{bat_ch}	Battery charging efficiency
η_{bat_d}	Battery discharging efficiency
$\rho_c(t)$	Aggregated internal resistance during charge (ΩAh)
$\rho_d(t)$	Aggregated internal resistance during discharge (ΩAh)
τ	Time between $t - \Delta t$ and t

References

- Salas, V.; Suponthana, W.; Salas, R.A. Overview of the off-grid photovoltaic diesel batteries systems with AC loads. *Appl. Energy* **2015**, *157*, 195–216. [\[CrossRef\]](#)
- Gomes, I.S.F.; Perez, Y.; Suomalainen, E. Coupling small batteries and PV generation: A review. *Renew. Sustain. Energy Rev.* **2020**, *126*, 109835. [\[CrossRef\]](#)
- Krieger, E.M.; Cannarella, J.; Arnold, C.B. A comparison of lead-acid and lithium-based battery behavior and capacity fade in off-grid renewable charging applications. *Energy* **2013**, *60*, 492–500. [\[CrossRef\]](#)
- Diouf, B.; Avis, C. The potential of Li-ion batteries in ECOWAS solar home systems. *J. Energy Storage* **2019**, *22*, 295–301. [\[CrossRef\]](#)
- García-Vera, Y.E.; Dufo-López, R.; Bernal-Agustín, J.L. Optimization of isolated hybrid microgrids with renewable energy based on different battery models and technologies. *Energies* **2020**, *13*, 581. [\[CrossRef\]](#)
- Svoboda, V.; Wenzl, H.; Kaiser, R.; Jossen, A.; Baring-Gould, I.; Manwell, J.; Lundsager, P.; Bindner, H.; Cronin, T.; Nørgård, P.; et al. Operating conditions of batteries in off-grid renewable energy systems. *Sol. Energy* **2007**, *81*, 1409–1425. [\[CrossRef\]](#)
- Lujano-Rojas, J.M.; Dufo-López, R.; Atencio-Guerra, J.L.; Rodrigues, E.M.G.; Bernal-Agustín, J.L.; Catalao, J.P.S. Operating conditions of lead-acid batteries in the optimization of hybrid energy systems and microgrids. *Appl. Energy* **2016**, *179*, 590–600. [\[CrossRef\]](#)
- Wenzl, H.; Baring-Gould, I.; Kaiser, R.; Liaw, B.Y.; Lundsager, P.; Manwell, J.; Ruddell, A.; Svoboda, V. Life prediction of batteries for selecting the technically most suitable and cost effective battery. *J. Power Sources* **2005**, *144*, 373–384. [\[CrossRef\]](#)
- Ekren, B.Y.; Ekren, O. Simulation based size optimization of a PV/wind hybrid energy conversion system with battery storage under various load and auxiliary energy conditions. *Appl. Energy* **2009**, *86*, 1387–1394. [\[CrossRef\]](#)
- McKenna, E.; McManus, M.; Cooper, S.; Thomson, M. Economic and environmental impact of lead-acid batteries in grid-connected domestic PV systems. *Appl. Energy* **2013**, *104*, 239–249. [\[CrossRef\]](#)
- Vasallo, M.J.; Bravo, J.M.; Andújar, J.M. Optimal sizing for UPS systems based on batteries and/or fuel cell. *Appl. Energy* **2013**, *105*, 170–181. [\[CrossRef\]](#)
- Huld, T.; Moner-Girona, M.; Kriston, A. Geospatial analysis of photovoltaic mini-grid system performance. *Energies* **2017**, *10*, 218. [\[CrossRef\]](#)
- Dolara, A.; Grimaccia, F.; Magistrati, G.; Marchegiani, G. Optimization Models for islanded micro-grids: A comparative analysis between linear programming and mixed integer programming. *Energies* **2017**, *10*, 241. [\[CrossRef\]](#)
- Ashtiani, M.N.; Toopshekan, A.; Astarai, F.R.; Yousefi, H.; Maleki, A. Techno-economic analysis of a grid-connected PV/battery system using the teaching-learning-based optimization algorithm. *Sol. Energy* **2020**, *203*, 69–82. [\[CrossRef\]](#)
- Say, K.; Schill, W.P.; John, M. Degrees of displacement: The impact of household PV battery prosumage on utility generation and storage. *Appl. Energy* **2020**, *276*, 115466. [\[CrossRef\]](#)
- Cho, D.; Valenzuela, J. Optimization of residential off-grid PV-battery systems. *Sol. Energy* **2020**, *208*, 766–777. [\[CrossRef\]](#)
- Aniello, G.; Shamon, H.; Kuckshinrichs, W. Micro-economic assessment of residential PV and battery systems: The underrated role of financial and fiscal aspects. *Appl. Energy* **2021**, *281*, 115667. [\[CrossRef\]](#)
- Jurasz, J.; Ceran, B.; Orłowska, A. Component degradation in small-scale off-grid PV-battery systems operation in terms of reliability, environmental impact and economic performance. *Sustain. Energy Technol. Assess.* **2020**, *38*, 100647. [\[CrossRef\]](#)
- Say, K.; John, M.; Dargaville, R. Power to the people: Evolutionary market pressures from residential PV battery investments in Australia. *Energy Policy* **2019**, *134*, 110977. [\[CrossRef\]](#)
- Chaianong, A.; Bangviwat, A.; Menke, C.; Breitschopf, B.; Eichhammer, W. Customer economics of residential PV-battery systems in Thailand. *Renew. Energy* **2020**, *146*, 297–308. [\[CrossRef\]](#)
- Dufo-López, R.; Bernal-Agustín, J.L. Design and control strategies of PV-diesel systems using genetic algorithms. *Sol. Energy* **2005**, *79*, 33–46. [\[CrossRef\]](#)
- Bernal-Agustín, J.L.; Dufo-López, R.; Rivas-Ascaso, D.M. Design of isolated hybrid systems minimizing costs and pollutant emissions. *Renew. Energy* **2012**, *44*, 215–224. [\[CrossRef\]](#)
- Dalton, G.J.; Lockington, D.A.; Baldock, T.E. Feasibility analysis of stand-alone renewable energy supply options for a large hotel. *Renew. Energy* **2008**, *33*, 1475–1490. [\[CrossRef\]](#)
- Bekele, G.; Palm, B. Feasibility study for a standalone solar-wind-based hybrid energy system for application in Ethiopia. *Appl. Energy* **2010**, *87*, 487–495. [\[CrossRef\]](#)
- Hlal, M.I.; Ramachandaramurthy, V.K.; Sarhan, A.; Pouryekta, A.; Subramaniam, U. Optimum battery depth of discharge for off-grid solar PV/battery system. *J. Energy Storage* **2019**, *26*, 100999. [\[CrossRef\]](#)
- Dufo-López, R.; Bernal-Agustín, J.L. Influence of mathematical models in design of PV-Diesel systems. *Energy Convers. Manag.* **2008**, *49*, 820–831. [\[CrossRef\]](#)

27. Bernal-Agustín, J.L.; Dufo-López, R. Multi-objective design and control of hybrid systems minimizing costs and unmet load. *Electr. Power Syst. Res.* **2009**, *79*, 170–180. [\[CrossRef\]](#)
28. Dufo-López, R.; Bernal-Agustín, J.L.; Yusta-Loyo, J.M.; Domínguez-Navarro, J.A.; Ramírez-Rosado, I.J.; Lujano, J.; Aso, I. Multi-objective optimization minimizing cost and life cycle emissions of stand-alone PV-wind-diesel systems with batteries storage. *Appl. Energy* **2011**, *88*, 4033–4041. [\[CrossRef\]](#)
29. Perera, T.D.; Attalage, R.A.; Perera, K.K.C.K.; Dassanayake, V.P.C. A hybrid tool to combine multi-objective optimization and multi-criterion decision making in designing standalone hybrid energy systems. *Appl. Energy* **2013**, *107*, 412–425. [\[CrossRef\]](#)
30. Schiffer, J.; Sauer, D.U.; Bindner, H.; Cronin, T.; Lundsager, P.; Kaiser, R. Model prediction for ranking lead-acid batteries according to expected lifetime in renewable energy systems and autonomous power-supply systems. *J. Power Sources* **2007**, *168*, 66–78. [\[CrossRef\]](#)
31. Dufo-López, R. iHOGA (improved Hybrid Optimization by Genetic Algorithms) Software. 2012. Available online: <https://ihoga.unizar.es/en> (accessed on 10 January 2021).
32. Ayeng'o, S.P.; Schirmer, T.; Kairies, K.P.; Axelsen, H.; Sauer, D.U. Comparison of off-grid power supply systems using lead-acid and lithium-ion batteries. *Sol. Energy* **2018**, *162*, 140–152. [\[CrossRef\]](#)
33. Dufo-López, R.; Lujano-Rojas, J.M.; Bernal-Agustín, J.L. Comparison of different lead-acid battery lifetime prediction models for use in simulation of stand-alone photovoltaic systems. *Appl. Energy* **2014**, *115*, 242–253. [\[CrossRef\]](#)
34. Armand, M.; Axmann, P.; Bresser, D.; Copley, M.; Edström, K.; Ekberg, C.; Guyomard, D.; Lestriez, B.; Novák, P.; Petranikova, M.; et al. Lithium-ion batteries—Current state of the art and anticipated developments. *J. Power Sources* **2020**, *479*. [\[CrossRef\]](#)
35. Zubi, G.; Dufo-López, R.; Carvalho, M.; Pasaoglu, G. The lithium-ion battery: State of the art and future perspectives. *Renew. Sustain. Energy Rev.* **2018**, *89*. [\[CrossRef\]](#)
36. Argyrou, M.C.; Christodoulides, P.; Kalogirou, S.A. Energy storage for electricity generation and related processes: Technologies appraisal and grid scale applications. *Renew. Sustain. Energy Rev.* **2018**, *94*, 804–821. [\[CrossRef\]](#)
37. Astaneh, M.; Roshandel, R.; Dufo-López, R.; Bernal-Agustín, J.L. A novel framework for optimization of size and control strategy of lithium-ion battery based off-grid renewable energy systems. *Energy Convers. Manag.* **2018**. [\[CrossRef\]](#)
38. Jafari, M.; Khan, K.; Gauchia, L. Deterministic models of Li-ion battery aging: It is a matter of scale. *J. Energy Storage* **2018**, *20*, 67–77. [\[CrossRef\]](#)
39. Astaneh, M.; Dufo-López, R.; Roshandel, R.; Bernal-Agustín, J.L. A novel lifetime prediction method for lithium-ion batteries in the case of stand-alone renewable energy systems. *Int. J. Electr. Power Energy Syst.* **2018**, *103*. [\[CrossRef\]](#)
40. Rechkemmer, S.K.; Zang, X.; Zhang, W.; Sawodny, O. Empirical Li-ion aging model derived from single particle model. *J. Energy Storage* **2019**, *21*, 773–786. [\[CrossRef\]](#)
41. Cortés-Arcos, T.; Dufo-López, R.; Bernal-Agustín, J.L. Estimating degradation costs for non-cyclic usage of lithium-ion batteries. *Appl. Sci.* **2020**, *10*, 5330. [\[CrossRef\]](#)
42. Oyarbide, M.; Arrinda, M.; Sánchez, D.; Macicior, H.; McGahan, P.; Hoedemaekers, E.; Cendoya, I. Capacity and impedance estimation by analysing and modeling in real time incremental capacity curves. *Energies* **2020**, *13*, 4855. [\[CrossRef\]](#)
43. Wang, J.; Liu, P.; Hicks-Garner, J.; Sherman, E.; Soukiazian, S.; Verbrugge, M.; Tataria, H.; Musser, J.; Finamore, P. Cycle-life model for graphite-LiFePO₄ cells. *J. Power Sources* **2011**, *196*, 3942–3948. [\[CrossRef\]](#)
44. Petit, M.; Prada, E.; Sauvart-Moynot, V. Development of an empirical aging model for Li-ion batteries and application to assess the impact of Vehicle-to-Grid strategies on battery lifetime. *Appl. Energy* **2016**, *172*, 398–407. [\[CrossRef\]](#)
45. Arnieri, E.; Boccia, L.; Amoroso, F.; Amendola, G.; Cappuccino, G. Improved efficiency management strategy for battery-based energy storage systems. *Electronics* **2019**, *8*, 1459. [\[CrossRef\]](#)
46. International Electrotechnical Commission. IEC 60896-1:1987 Stationary Lead-Acid Batteries. General Requirements and Methods of Test. Vented Types; International Electrotechnical Commission: Geneva, Switzerland, 1987.
47. Downing, S.; Socie, D. Simple Rainflow Counting Algorithms. *Int. J. Fatigue* **1982**, *4*, 31–40. [\[CrossRef\]](#)
48. Commercial OPzS Battery. Available online: http://inversolar.es/wp-content/uploads/2019/12/EN-PS-TS-RS-005_0814.pdf (accessed on 17 January 2021).
49. Shepherd, C.M. Design of primary and secondary cells II. An equation describing battery discharge. *J. Electrochem. Soc.* **1965**, *112*, 657. [\[CrossRef\]](#)
50. Groot, J.; Swierczynski, M.; Stan, A.I.; Kaer, S.K. On the complex ageing characteristics of high-power LiFePO₄/graphite battery cells cycled with high charge and discharge currents. *J. Power Sources* **2015**, *286*, 475–487. [\[CrossRef\]](#)
51. Naumann, M.; Schimpe, M.; Keil, P.; Hesse, H.C.; Jossen, A. Analysis and modeling of calendar aging of a commercial LiFePO₄/graphite cell. *J. Energy Storage* **2018**, *17*, 153–169. [\[CrossRef\]](#)
52. European Commission, PVGIS. 2020. Available online: <https://ec.europa.eu/jrc/en/pvgis> (accessed on 13 September 2020).